

Wide-Angle Michelson Interferometer for Measuring Doppler Line Widths*

R. L. HILLIARD† AND G. G. SHEPHERD

Institute of Upper Atmospheric Physics, University of Saskatchewan, Saskatoon, Canada

(Received 30 July 1965)

The field-compensation principle, which has been applied to interferometric spectroscopy independently by P. Connes and by L. Mertz, allows the useful solid angle accepted by an interferometer to be increased by an amount that can be very large. This paper is concerned with a particular application of this principle using the Michelson interferometer. Although the technique is difficult to utilize where a wide range of path differences is required, the interferometer takes an extremely simple form when constructed for a narrow range of path difference about a fixed central path difference. While such an instrument has a limited use in spectroscopy, there is one type of measurement which it is admirably suited to perform: the determination of the width of a single isolated atomic line whose analytical shape is known. A description is given of the theory and construction of a wide-angle Michelson interferometer now being used for the measurement of Doppler temperatures from the width of the 5577 Å atomic oxygen line in the nightglow and aurora. This line is known to be accurately gaussian in shape, and is well-isolated from other lines, making it an ideal subject for this instrument.

INDEX HEADINGS: Interferometer; Spectroscopy; Doppler effect.

1. INTRODUCTION

INTERFEROMETRIC spectroscopy is becoming increasingly common, particularly in those laboratories where the experiments are limited by the source brightness. This is because of the general recognition that with interferometric devices, a greater photon flux is delivered to the detector for a given source radiance and spectral resolution. Jacquinot¹, who first pointed this out, used the word luminosity to describe this characteristic. Since that word has another meaning, we use radiance response here instead, and mean by it the photon flux delivered to the detector divided by the source radiance.

Of the various interferometers, that of Fabry and Perot has perhaps been the most widely used so far, despite the limitation of its multiple passbands. But this limitation can be overcome with multiple étalon systems; successful tandem instruments have been constructed.²⁻⁴ The other important spectroscopic interferometer is that of Michelson; it has been success-

fully employed by several users.⁵⁻⁸ Its great flexibility is achieved at the cost of having to compute numerical Fourier transforms.

The ingenious SISAM,⁹ and the multislit spectrometer¹⁰ have not yet been much used, although Tinsley¹¹ has recently described a promising form of the latter instrument. For a review of this field, readers are referred to the paper by Jacquinot,¹² then director of the laboratory responsible for many of the recent developments in interferometric spectroscopy.

At Saskatoon, spectroscopic measurements of upper atmospheric temperature have been carried out for many years, in particular, rotational temperature measurements from molecular bands.¹³ Most recently, two series of Doppler temperature measurements in aurora were made with a Fabry-Perot spectrometer.^{14,15}

With the latter, Doppler temperatures having a probable error of 50K° were obtained from weak

* Presented at the Spring Meeting of the Optical Society of America in Dallas, 2 April 1965. *J. Opt. Soc. Am.* **55**, 615A (1965).

† Present Address: Steward Observatory, University of Arizona, Tucson, Arizona 85721.

¹ P. Jacquinot, *J. Opt. Soc. Am.* **44**, 761 (1954).

² R. Chabbal, Thèses, Université de Paris, 1958.

³ J. E. Mack, D. P. McNutt, F. L. Roesler, and R. Chabbal, *Appl. Opt.* **2**, 873 (1963).

⁴ G. G. Shepherd, C. W. Lake, J. R. Miller, and L. L. Cogger, *Appl. Opt.* **4**, 267 (1965).

⁵ P. Fellgett, *J. Phys. Radium* **19**, 237 (1958).

⁶ J. Connes, *J. Phys. Radium* **19**, 197 (1958).

⁷ H. A. Gebbie, *J. Phys. Radium* **19**, 230 (1958).

⁸ J. Connes and H. Gush, *J. Phys. Radium* **20**, 915 (1959).

⁹ P. Connes, *J. Phys. Radium* **19**, 215 (1958).

¹⁰ A. Girard, *Appl. Opt.* **2**, 79 (1963).

¹¹ B. A. Tinsley, *J. Opt. Soc. Am.* **55**, 599A (1965).

¹² P. Jacquinot, *Rep. Progr. Phys.* **23**, 267 (1960).

¹³ D. M. Hunten, *Ann. Geophys.* **17**, 249 (1961).

¹⁴ J. A. Nilson and G. G. Shepherd, *Planetary Space Sci.* **5**, 299 (1961).

¹⁵ E. C. Turgeon and G. G. Shepherd, *Planetary Space Sci.* **9**, 295 (1962).

auroras using scanning times of about 15 secs. A double-étalon instrument has subsequently been used for dayglow observations.¹⁶ Although the Fabry-Perot spectrometer has been very useful, a substantially greater radiance response is desirable to permit observations of time-dependent auroral phenomena, as well as fainter emissions such as nightglow.

The ordinary Michelson interferometer yields the same radiance response as the Fabry-Perot spectrometer; it therefore offers no advantages for this particular application. However, the useful field of the Michelson interferometer may be widened (or compensated), as shown originally by Hansen¹⁷⁻¹⁹ and described later by Connes²⁰ and Mertz,²¹ by making the path difference of the interferometer a slowly varying function of incidence angle. The gain of radiance response over that of the uncompensated instrument increases with the path difference used; for line-width studies it will be demonstrated that gains of about one thousand are possible in principle. Field compensation of the Fabry-Perot spectrometer can be accomplished with spherical plates,²² but the resulting gain is significant only at resolving powers much greater than those required for these measurements.

We therefore directed our attention to the Michelson interferometer. A very simple arrangement provides correct field compensation for a given path difference. This makes the device highly suitable for Doppler line-width measurements because the width of an isolated line of known shape may be determined by observing the fringe modulation over a single order of interference at a particular path difference. Moreover, this may be done without numerical Fourier transformation.

The following sections of this paper contain: a discussion of the method for determining a line width from the modulation obtained over a very narrow range of path difference centered at some particular path difference, a simple explanation of the field-compensation principle, a more detailed analysis, and finally a description of the instrument and some sample results. Because the term "compensation" can be applied to the interferometer in both the spatial and the spectral sense, this term is avoided in this paper; the term Wide Angle Michelson Interferometer (WAMI) is used instead, and the symbol MI used for the ordinary instrument.

¹⁶ A. R. Bens, L. L. Cogger, and G. G. Shepherd, *Planetary Space Sci.* **13**, 551 (1965).

¹⁷ G. Hansen, *Optik* **12**, 5 (1955).

¹⁸ G. Hansen and W. Kinder, *Optik* **15**, 560 (1958).

¹⁹ The authors are indebted to Dr. W. H. Steel for drawing these references to their attention.

²⁰ P. Connes, *Rev. Opt.* **35**, 37 (1956).

²¹ L. Mertz, preprints of papers presented at the Fifth Meeting and Conference of the I. C. O., Stockholm, Aug. 1959. Ed.: E. Ingelstam.

²² P. Connes, *J. Phys. Radium* **19**, 262 (1958).

2. MEASUREMENT OF DOPPLER LINE WIDTH WITH A MICHELSON INTERFEROMETER

As is well-known, the variable part of the interferogram produced as the interferometer scans is the Fourier transform of the source spectrum.¹² We are here concerned with a source spectrum that is an isolated gaussian line centered at wavenumber σ_0 . The differential source radiance as a function of wavenumber σ is given by

$$B\sigma B_0 \exp[-(\sigma - \sigma_0)^2 4 \ln 2 / w^2], \quad (1)$$

where w is the half-intensity width of the line, which in the case of purely Doppler broadening can be related to the source temperature T by,

$$w = (7.16 \times 10^{-7}) \sigma_0 (T/M)^{1/2}, \quad (2)$$

where T is in °K and M is the mass of the atomic species in amu.

The Fourier transform of a gaussian of width w centered at σ_0 in "σ space" is, in "path-difference space" a gaussian of half-intensity width $(4 \ln 2)^{1/2} / (\pi^2 w^2)$, centered at a path difference $\Delta = 0$, and multiplied by $\cos 2\pi\sigma_0\Delta$. This result was worked out explicitly by Michelson.²³ As pointed out by Jacquinot,¹² the gaussian envelope is very conveniently identified with Michelson's concept of fringe visibility. Accordingly, by making use of Eq. (2), we can express the visibility as

$$V = \exp[-QT\Delta^2], \quad (3)$$

where

$$Q = ((7.16)^2 \times 10^{-14} / 4 \ln 2) (\pi^2 \sigma_0^2 / M). \quad (4)$$

For the 5577-Å line of atomic oxygen, Eq. (4) becomes

$$Q = 3.66 \times 10^{-5} \text{ } ^\circ\text{K}^{-1} \text{ cm}^{-2}. \quad (5)$$

It is thus seen that a measurement of V leads directly to the determination of temperature T , assuming, of course, that the interferometer and source are perfect. Techniques for removing the necessity for these assumptions are discussed later.

3. THE FIELD-COMPENSATION PRINCIPLE

The field-compensation principle can be explained simply by referring to Fig. 1, in which a conventional MI is shown, and Fig. 2 in which the WAMI is shown. In Fig. 1 the movable mirror M_2 is shown in two positions. Position 1, where M_2 is coplanar with the image M_1' of M_1 , corresponds to zero path difference, and position 2, where M_2 is parallel to but not coplanar with M_1' , corresponds to some finite path difference. The path of an off-axis ray through the system is shown. For position 1, the divided rays, after recombination, emerge collinearly from the instrument. For position 2, the two ray components have a relative displacement.

²³ A. A. Michelson, *Studies in Optics*, (University of Chicago Press, Chicago, 1927).

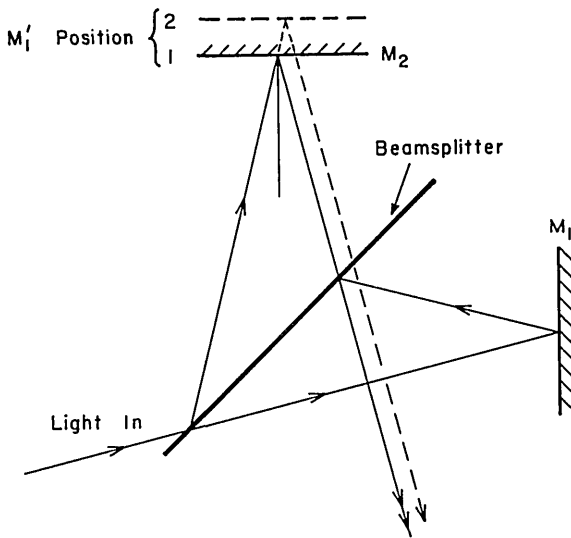


FIG. 1. The conventional Michelson interferometer. Position 1 of M_1' is for zero path difference, and the emergent rays are collinear. Position 2 corresponds to a nonzero path difference, and the emergent rays have a relative displacement.

It follows that for position 1 the path difference is zero regardless of the angle of incidence (because the ray paths form identical triangles on both sides of the beamsplitter), whereas in position 2 the path difference becomes a function of the angle. In short, it can be said that an MI with zero path difference is a perfectly field-compensated instrument.

In Fig. 2 the mirror M_2 has been replaced by a back-aluminized plane-parallel glass slab. This slab is so placed that the virtual image of its back face coincides with M_1' . The result is that the ray components emerge

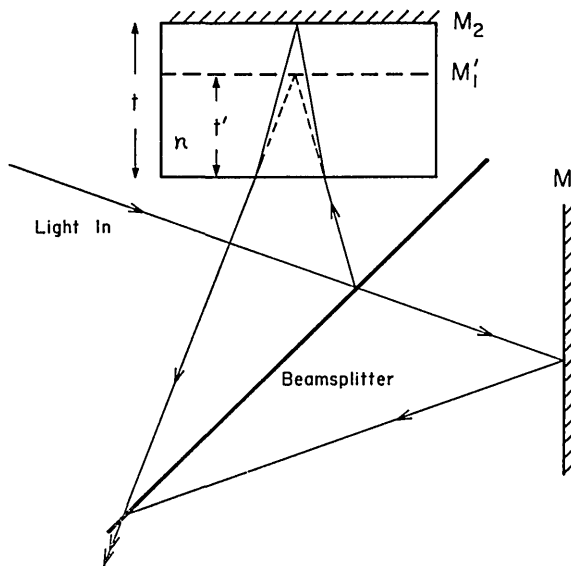


FIG. 2. Wide-angle Michelson interferometer. The front-surfaced mirror M_2 has been replaced by a back-surfaced slab of refractive index n . The dotted line indicates the apparent path of the ray in the slab as reflected from the virtual image of M_2 . Although there is a nonzero path difference, the emergent rays are collinear.

collinearly from the instrument (to the approximation that the position of M_1' is independent of incidence angle). But the path difference is not zero, since the travel time for light in the path containing the slab is longer than in the path in air.

This effect can be readily verified experimentally by observing the fringes produced by a narrow-line source with the above arrangement. As the path difference for which the above condition occurs is approached, the fringes expand and the visibility becomes large just as happens near zero path difference in the MI. In other words, some of the zero path characteristics of the MI appear at some particular nonzero path difference in the WAMI; that path difference shall be referred to as the quasi-zero path difference, abbreviated QZP.

For normally incident light Fig. 2 shows that the

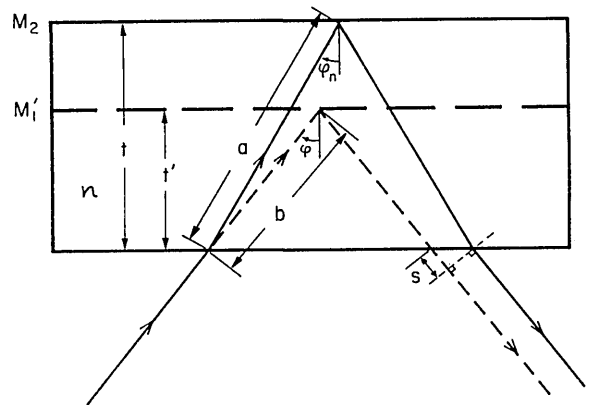


FIG. 3. Showing the geometry of the reflection in the slab in detail. The path in glass is indicated by the solid line, and the superimposed path in air is shown as the dotted line.

path difference is equal to $2nt - 2t'$, where t is the thickness of the slab, t' is the apparent distance to the virtual image of the back surface, and n is the refractive index of the slab. It will be seen later that it is difficult to define a physically meaningful QZP condition precisely; for convenience and simplicity we shall say that the QZP condition occurs when t' is equal to t/n . The path difference for normal incidence at the QZP condition is thus given by

$$\Delta_0(\text{QZP}) = 2(nt - t/n). \tag{6}$$

4. CALCULATION OF THE VARIATION OF PATH DIFFERENCE WITH ANGLE

Because the position of M_1' varies with incident angle, perfect field compensation is not possible. A more precise analysis is required to determine the limits of this compensation. The path difference for an off-axis ray may be calculated by reference to Fig. 3. This figure is an elaboration of Fig. 2 but shows the paths only near the mirrors M_1 and M_2 . The two paths are shown superimposed, with the dotted line representing the path which is in air. The case considered is one in

which the image M_1' does not coincide with the virtual image of M_2 but is located close to it. Using the notation of the Figure and recalling that the ray shown as solid is in glass of refractive index n and that the path shown dotted is in air, we find the path difference:

$$\Delta = 2na - 2b - s. \quad (7)$$

The path segments a , b , and s are given by,

$$a = t/\cos\varphi_n, \quad b = t'/\cos\varphi, \quad (8)$$

and

$$s = 2 \sin\varphi(t \tan\varphi_n - t' \tan\varphi). \quad (9)$$

As shown in Fig. 3, t and φ_n are, respectively, the slab thickness and ray angle with the normal for the path in glass, while t' and φ are the analogous quantities for the path in air. Substituting Eq. (8) and Eq. (9) into Eq. (7) and using Snell's law, we obtain,

$$\Delta = 2(tn \cos\varphi_n - t' \cos\varphi). \quad (10)$$

When $\varphi = 0$ and t' is set equal to t/n , Eq. (10) reduces to Eq. (6).

The significance of Eq. (10) is not obvious at first sight. It is instructive to calculate the change in path difference with angle for the situation where $t' = t/n$; that is, to subtract Eq. (6) from Eq. (10). If we do this, using approximations adequate for the Fabry-Perot or Michelson interferometers ($\sin\theta = \theta$, and $\cos\theta = 1 - \theta^2/2$), we obtain $\Delta - \Delta_0 = \theta$. Thus, to this degree of approximation, the compensation is perfect and the path difference is completely independent of the incidence angle.

This idea can be expressed formally by writing $\Delta - \Delta_0$ in a power series in φ as follows:

$$\Delta - \Delta_0 = A\varphi + B\varphi^2 + C\varphi^3 + D\varphi^4 + E\varphi^5 + \dots \quad (11)$$

This equation applies to all spectrometers or interferometers; for example, a grating spectrometer with normally incident light has $\Delta - \Delta_0 = 2t \sin\varphi \cong 2t\varphi$. Thus for a grating spectrometer (since $\varphi \ll 1$) the dominant term in Eq. (11) is $A\varphi$ and the additional terms are needed only for higher-order approximations (B , D etc. are equal to zero but that is not important here). For the Fabry-Perot and Michelson interferometers we have $\Delta - \Delta_0 = -2t(1 - \cos\varphi)$, which when expanded gives $A = 0$ with $B\varphi^2$ the dominant term. This cancellation of the $A\varphi$ term gives the MI its advantage over the grating spectrometer.²⁴ Expressed in this way the advantage of the WAMI over the MI arises from the cancellation of the $B\varphi^2$ term, and as shown below, the $C\varphi^3$ term as well.

To investigate in more detail the variation of path difference with angle, higher powers of φ must be used. In addition, the restriction that t' be equal to t/n need not be imposed; small deviations from the

QZP condition are expressed as the small quantity e , where

$$t' = t/n + e. \quad (12)$$

Using Snell's law and expanding the cosine to the fourth order, we obtain

$$\cos\varphi_n = (1/n)[n^2 - \varphi^2 + \varphi^4/3]^{1/2}. \quad (13)$$

If we expand Eq. (13) in a binomial expansion, expand $\cos\varphi$ to fourth order, substitute in Eq. (10), and use Eq. (6), the result is

$$(\Delta - \Delta_0)_{\text{WAMI}} = e\varphi^2 + (t/4n^2)(n - 1/n)\varphi^4. \quad (14)$$

By making use of Eq. (6), we can write this as

$$(\Delta - \Delta_0)_{\text{WAMI}} = e\varphi^2 + \Delta_0\varphi^4/8n^2. \quad (15)$$

The analogous equation for the MI is

$$(\Delta_0 - \Delta)_{\text{MI}} = \Delta_0\varphi^2/2 - \Delta_0\varphi^4/24. \quad (16)$$

Comparison of Eqs. (15) and (16) shows how closely e , the distance from the QZP condition, is analogous to $\Delta_0/2$ for the MI. Returning to Eq. (11), we now see that the advantage of the WAMI is that e can be set equal to zero at any path difference, eliminating all terms up to $D\varphi^4$, whence Eq. (14) reduces to

$$(\Delta - \Delta_0)_{\text{WAMI}} \cong \Delta_0\varphi^4/8n^2. \quad (17)$$

This approximate equation is simple and often convenient to use for the WAMI. But it is conservative, because Eq. (15) is still the accurate equation and as is shown in the next section, the use of negative e values permits a partial cancellation of the terms in φ^2 and φ^4 , and makes it possible to use off-axis angles even greater than indicated by Eq. (17).

5. REDUCTION IN OBSERVED FRINGE VISIBILITY RESULTING FROM A FINITE APERTURE

It is clear that for a perfectly monochromatic source and a pinhole aperture, $V = 1$, but that as the aperture is made finite, the superposition of fringes of varying Δ causes the visibility to decrease to a value that we shall call the aperture visibility parameter, denoted by V_a . Unlike the case for the MI,⁶ the treatment of this effect for the WAMI does not lend itself to analytical methods. A numerical treatment is described in what follows.

The case for $e = 0$ is considered first. The aperture may be divided into annular segments, each of which has a path difference that differs from that of its immediate neighbors by the same amount $d\Delta$. The contribution to the interferogram from a single segment can be represented by a vector with amplitude proportional to the area of the segment, and phase angle $2\pi(\Delta - \Delta_0)/\lambda$ corresponding to the value of $(\Delta - \Delta_0)$ for that segment. The situation is as pictured in the inset of Fig. 4. From the inset it can be seen that the segment

²⁴ Of course, for a grating spectrometer, the angle φ determines only the slit width; the slit length must also be considered in comparing the two instruments.

area is proportional to $\varphi d\varphi$, which from Eq. (17) is related to $d\Delta$ by

$$\varphi d\varphi = n[1/2(\Delta - \Delta_0)\Delta_0]^{1/2} d\Delta. \quad (18)$$

In writing this in terms of phase angles rather than path differences we replace $d\Delta$ by $\lambda\delta/2\pi$, where δ is the constant incremental phase angle, Δ_0 by $\lambda\delta_0/2\pi$, and $\Delta - \Delta_0$ by $\lambda N\delta/2\pi$, where N is an integer giving the number of the segment (increasing outward from $N=1$ at the center to $N=M$ at the edge of the aperture). Thus Eq. (18) is replaced by

$$\varphi d\varphi = n(\delta/2N\delta_0)^{1/2}. \quad (19)$$

Since δ_0 and δ are constant, the intensity amplitude vector is proportional to $1/N^{1/2}$. The contribution to the interferogram can be expressed in arbitrary units as

$$A \exp(i\alpha) = 1 + 1^{-1/2} \exp(i\delta) + 2^{-1/2} \exp(i2\delta) + \dots + M^{-1/2} \exp(iM\delta). \quad (20)$$

The x and y components of the vector $A \exp(i\alpha)$ were calculated separately; the results of this calculation are shown in Fig. 4, where the y component of A has been plotted against its x component for M increasing from 1 to 100 and $\delta = 0.1$ rad. A smooth curve has been drawn through the points. Some values of $\Delta - \Delta_0$ (in 5577-Å radiation wavelengths) and of φ_M (φ_M is the value of φ for the edge of the aperture) for the authors' instrument ($\Delta_0 = 5.2$ cm) are indicated at intervals along the curve. However, this curve could be adapted for any other such instrument. As φ increases the magnitude A increases and its phase α changes. The visibility parameter V_a is given by the vector magnitude of any point on the curve, divided by the arc length from the origin to that point. Before presenting results of the calculation of V_a , we will make the extension to the general case ($e \neq 0$).

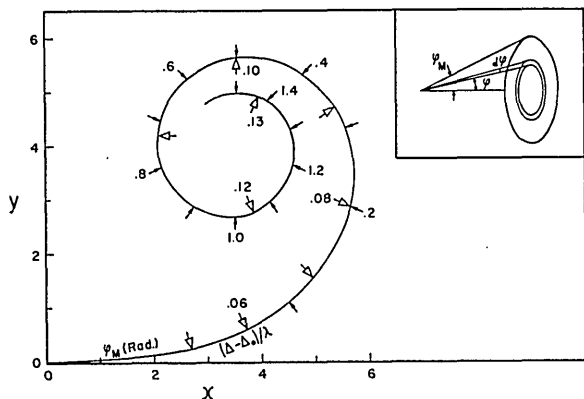


FIG. 4. Showing the effect of a finite aperture on the WAMI. The geometry is shown in the inset. The spiral is the locus of the tip of a vector representing the intensity and phase of the fringes transmitted by the aperture. Moving up the spiral corresponds to opening up the aperture. The aperture half-angle φ_m is shown in radians by the open arrows. The change in path difference from the center of the aperture to its edge is indicated, in wavelengths, by the solid arrows. The spiral is drawn for a path difference of 5.0 cm and a wavelength of 5577 Å

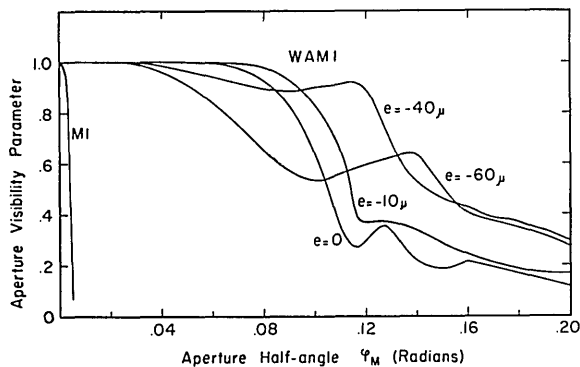


FIG. 5. Showing how the aperture visibility parameter V_a changes with aperture half-angle φ_m for various values of $e = l' - l/n$. e is the displacement from the normal incidence QZP condition. The path difference is 5 cm. The curve marked MI is for a conventional Michelson interferometer.

The procedure used for $e \neq 0$ was similar to that described above, except that the segments used had not equal phase width but equal angular widths $d\varphi$, instead. For each segment, the area was simply $\varphi d\varphi$ and Eq. (14) was used to calculate its phase angle. The results of this calculation are shown in Fig. 5 as visibility parameter versus φ_M for various e , and in Fig. 6 as visibility parameter versus e for various φ_M . From Fig. 5 it is seen that for $e=0$, V_a is very close to unity up to $\varphi_M=0.06$ rad, after which it drops rapidly. (The curve for a MI is shown on the same graph.) For negative values of e , V_a departs from unity for smaller values of φ_M , but increases again at larger φ_M . For example, for $e=-40 \mu$, $V_a=0.9$ can be obtained at $\varphi_M=0.12$ rad, giving a fourfold increase in radiance response for only a moderate loss of visibility. On the other hand, Fig. 6 shows that as φ_M is increased, the range of e over which V_a remains near unity is much reduced, making the mirror location more critical.

6. RADIANCE RESPONSE AND RESOLVING POWER OF THE WAMI

Resolving power of a spectral device indicates an instrument's ability to isolate a spectral feature from its companions. In this context the concept is relatively unambiguous. But in certain specialized studies one is more concerned with the ability of an instrument to reproduce accurately a particular characteristic of a spectral-distribution function; for example, the width of a single gaussian line. Though a criterion might be invented to describe this ability, in principle this characteristic can be extracted from a smeared record with perfect accuracy once the instrumental characteristics are known perfectly. For a noiseless record, this would yield infinite resolution in this spectral characteristic. In practice, noise is always present and the effective resolving power becomes a function of the signal-to-noise ratio, and therefore cannot be assigned a fixed value.

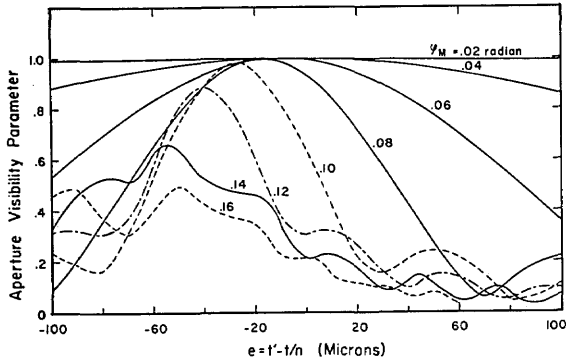


Fig. 6. The same data as in Fig. 5, plotted to show the variation of V_a with e for various φ_m .

If this is true for an instrument whose output is a spectrum, it is much more true for the WAMI as used here, for which the theoretical output is a function only of the path difference and the width of the gaussian line source. In the presence of noise the accuracy of the WAMI is optimized by choosing the path difference which gives the greatest sensitivity of visibility to source temperature; that is, one which yields the maximum value for dV/dT . Using Eq. (2) and Eq. (3) to calculate $(d/d\Delta)(dV/dT)$, we find that for a given line width w , the path difference Δ_W which gives dV/dT its maximum value occurs when

$$w\Delta_W = 2(\ln 2)^{1/2} / \pi \cong 0.5. \quad (21)$$

This relation can be used to define a resolving power for the WAMI by saying that if the WAMI is set to a path difference Δ_W , it has a resolving power $R_{WAMI} = \sigma/w$, where w is the line width given by Eq. (21). With this definition, w is not to be thought of as the narrowest width the instrument can measure, but the optimum one.

Combining Eq. (21) with this definition we get

$$R_{WAMI} = \sigma\pi\Delta_W / 2(\ln 2)^{1/2} \cong 2\sigma\Delta_W. \quad (22)$$

Using the definition of resolving power for the scanning MI, where now Δ_M is the maximum path difference, we obtain a remarkably similar equation,

$$R_{MI} = 2\sigma\Delta_M. \quad (23)$$

In other words, when Δ_W is set equal to Δ_M , the resolving power of the WAMI as defined is equal to the resolving power of the MI.

The photon flux transmitted by the interferometer is given by

$$F = S\Omega\tau B, \quad (24)$$

where S is the area of the limiting element, Ω is the solid angle accepted by S , τ is the transmittance of the instrument, and B is the radiance of the extended source in photons $\text{cm}^{-2} \text{sec}^{-1} \text{sr}^{-1}$. The radiance response (sometimes called light-gathering power and sometimes called throughput) is proportional to $S\Omega\tau$.

The quantity $S\Omega$ is called *étendue* in French, and has been translated by some as light grasp, by others as flux acceptance. (This confusion in terminology has been pointed out elsewhere.⁴) The quantity Ω , the solid angle of acceptance, is here called the angular acceptance. Since $\Omega \cong \pi\varphi_M^2$, it is clear from Fig. 5 that the WAMI is an instrument of great angular acceptance. Even though it is used here as a high-resolution device, the useful angle accepted by it is comparable to that which can be accepted by a low-resolution device such as an interference filter. For example, the OI nightglow emission at 5577 Å has a B of about 2×10^7 photons $\text{cm}^{-2} \text{sec}^{-1} \text{sr}^{-1}$; therefore for typical values of $S = 20 \text{ cm}^2$, $\tau = 0.1$, and $\varphi_M = 0.05 \text{ rad}$, a flux of about 0.75×10^8 photons/sec is obtained, which is readily measured with a photomultiplier.

Since it has already been shown that the WAMI and MI have equal "resolutions" when the fixed path difference for the former is equal to the maximum path difference for the latter, the angular acceptances for the two devices can be compared by calculating the ratio of φ_M^2 for the two instruments when both path differences are equal. An approximate analytical expression can be obtained by using Eqs. (16) and (17) and neglecting the φ^3 term for the MI. The result is,

$$(\varphi_M^2)_{WAMI} / (\varphi_M^2)_{MI} = [2n^2\Delta_0 / (\Delta - \Delta_0)]^{1/2}, \quad (25)$$

which, using either Eqs. (22) or (23), and taking $\Delta - \Delta_0 = 0.5$, we find to be

$$(\varphi_M^2)_{WAMI} / (\varphi_M^2)_{MI} = 2n(R)^{1/2}. \quad (26)$$

The gain of the WAMI over the MI increases as the square root of the resolving power, and it is now clear why for the application discussed in this paper the WAMI shows up so favorably.

Since the assumptions made in arriving at the above result may be criticized as being somewhat arbitrary, it may be worthwhile to make a more direct comparison for one particular case. This can be done by using the results of Fig. 5 to compare φ_M^2 for the WAMI and MI when both are set to the same path difference of 5 cm and both are used in the same way (measurement of visibility at a single path difference). If we make the comparison for $V_a = 0.9$ for both instruments the result is $(\varphi_M^2)_{WAMI} / (\varphi_M^2)_{MI} = 1.2 \times 10^3$, which is very close to the result obtained by using Eqs. (22) and (26).

7. REDUCTION IN FRINGE VISIBILITY RESULTING FROM INSTRUMENTAL IMPERFECTIONS

In a real interferometer, the surfaces are neither perfectly flat nor perfectly smooth, nor are they always in optimum adjustment. Furthermore, the reflectances of the beamsplitter and front- and back-surfaced mirrors are such that the two beams cannot be perfectly balanced. All of these effects combine to make the visibility less than unity for perfectly monochro-

matic light and $\varphi_M \rightarrow 0$. Let the measured visibility under such conditions be called the imperfection visibility parameter, denoted by V_i . Then for a real source and a real instrument, we can write, using Eq. (3),

$$V_{\text{obs}} = V_a V_i e^{-Q T \Delta^2} \quad (27)$$

A line source of known visibility, such as a ^{198}Hg lamp can be used to determine the quantity $V_a V_i$. If $V_a V_i$ were measured as $\varphi_M \rightarrow 0$ then V_a and V_i could be determined separately for any φ_M , but there is no necessity for this in the present application and it was not done. In any event, since a rather small φ_M of 0.05 rad was used, V_a was essentially unity.

8. THE EFFECT OF DISPERSION

The MI is normally used in a dispersion-compensated arrangement, but it is apparent that dispersion compensation and field compensation are mutually exclusive. This means that the field compensation can be maintained over only a limited range of wavelengths. The change in path difference $d\Delta$, arising from dispersion for a wavelength change $d\lambda$, is obtained by differentiating Eq. (10) with t' fixed and φ_n equal to zero, giving

$$d\Delta/d\lambda = 2tdn/d\lambda. \quad (28)$$

For a spectral line width of 0.02 \AA , $t=3 \text{ cm}$, and borosilicate crown glass at 5577 \AA , the path-difference shift is about 10^{-2} wavelengths, which is just small enough to be ignored in the present application. But for much broader lines, or at wavelengths near the ultraviolet cutoff of the glass, the effect would be important and would have to be considered.

9. DESCRIPTION OF THE CONSTRUCTED INSTRUMENT

A WAMI was constructed by the authors for the specific purpose of measuring Doppler line widths of emission lines of the upper atmosphere. The optical geometry of the interferometer is shown in Fig. 7. The beamsplitter substrate and compensating medium are provided by a pair of 90° prisms. The dimensions of the prisms are such that together they form a cube that is 6 cm on each side. A layer of rhodium is deposited on the hypotenuse of one of the prisms to form the semireflecting beamsplitter.²⁵

The optical flatness of all the critical surfaces (indicated by heavy lines) was $\lambda/20$. The two hypotenuses were wrung to provide a strong bond without the use of an adhesive.

The back-surface mirror (M_2) was deposited on a plane-parallel glass slab. This had a physical thickness of 3 cm and was 6 cm square. The front face of the slab was pressed against one of the prisms, with an

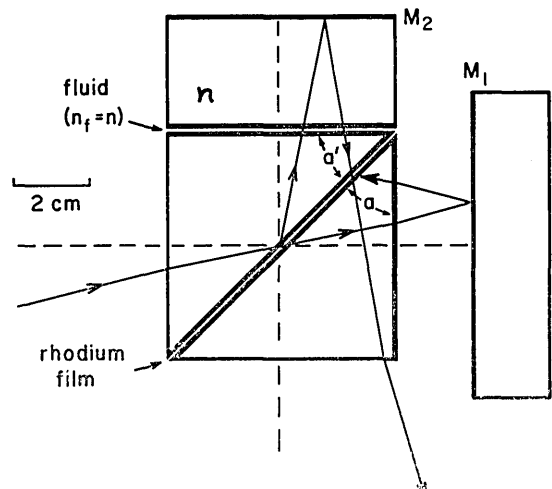


FIG. 7. Showing the configuration of the optics used for the constructed instrument.

intervening layer of oil having a refractive index matching that of the glass.

This type of optical geometry has a number of advantages over the conventional arrangement, which uses four mechanically independent optical components (the two mirrors, beamsplitter substrate, and compensating plate). This geometry creates virtually a two-component interferometer; the only significant instability is between the front-surfaced mirror (M_1) and the remainder of the optics. The beamsplitter is protected to such a degree that it is essentially permanent. For the WAMI, the large off-axis angles can cause considerable vignetting unless the beamsplitter is much larger than the other mirrors. In the split-cube arrangement the sizes of the beamsplitter, as well as the sizes of the other critical surfaces, are reduced by the order of 30%, compared to the conventional arrangement. This results in a more compact instrument and a reduction in the cost of the optics.

The angles a and a' were made very nearly equal (in our case they were the same to better than a second of arc, although a difference somewhat larger than this could probably be tolerated). This was to insure that the fringes were not distorted when large fields were used. Small differences could have been corrected by making the thin oil layer assume the proper wedge shape; but this correction was not found necessary.

The WAMI was operated exclusively in a narrow path-difference region near 5.2 cm. It would have been possible to use a mechanical motion to set the mirror M_1 position for the compensation and then use a limited scanning-range technique (e.g. refractive index or piezoelectric) to scan over the single fringe required. However, a single mechanical bearing was used to accomplish both purposes. With this type of scanning it proved more efficient to scan over a few hundred orders before recycling M_1 . The angle of the cone ($2\varphi_M$) accepted by the WAMI was set at 0.1 rad to

²⁵ The assembly was fabricated by Hilger and Watts, Inc.

ensure that V_a did not depart significantly from unity over this range.

In practice, particularly for faint sources such as nightglow, there is a significant amount of continuous background radiation which must be extracted from the data before the analysis is done. One way to avoid this problem would be to measure V for two different path differences (one of which could conveniently be very close to zero) and to use the ratio of these values to calculate T . For continuous measurement, this procedure would require two independent instruments. If these two instruments had the same V_i , then this technique would eliminate the need to determine V_i and would also eliminate the continuum radiation. Since this would be both expensive and difficult to achieve, the much simpler auxiliary interference-filter photometer was used. The passband of the interference filter

was shifted from that used in the interferometer so that it had essentially the same transmittance for the background. This photometer supplied a balance signal which was electronically subtracted from the interferometer signal to obtain the desired correction.

The details of the balancing procedure and other experimental details pertaining specifically to the air-glow and aurora are described in the paper containing the results of the observations.²⁶

10. DISCUSSION

Some sample results are shown in Fig. 8. For auroras the signal-to-noise ratio is very good; even for nightglow it is entirely satisfactory. Comparison with earlier results obtained with a Fabry-Perot spectrometer^{14,15} indicates that the improvement is indeed significant.

It may be concluded that the light-gathering capabilities of the WAMI exceed that of the MI by a large amount, provided that attention is paid to the parameters discussed in detail in the paper. To utilize this great capability in line-width determinations it is necessary to consider three factors. First, a line shape (preferably analytical) must be assumed for the emission. Second, a source of known V must be available. Finally, all other radiations must be excluded, or, in the case of background continuum, a suitable correction must be made. Which of these three factors will be limiting depends on the particular problem at hand. The first is undoubtedly the most fundamental limitation, but observations at several different path differences could make this limitation less severe. The third factor is the most important from an experimental point of view, but narrow-band interference filters greatly reduce the seriousness of this as a limiting factor.

ACKNOWLEDGMENTS

The preliminary ideas underlying the technique described in this paper first arose during a three-month visit by one of the authors (G. G. S.) to the Laboratoire Aimé Cotton, Bellevue, France in 1961. He wishes to express his appreciation to Dr. P. Jacquinot, Dr. R. Chabbal, and Dr. P. Connes for hospitality extended at that time. Financial support for that visit, as for all research described here, was provided by the National Research Council of Canada.

Dr. D. M. Hunten kindly read the manuscript and made helpful suggestions, as did Dr. H. P. Gush. The computer programs were written by Marian M. Shepherd.

²⁶ R. L. Hilliard and G. G. Shepherd, *Planetary Space Sci.* (to be published, 1966).

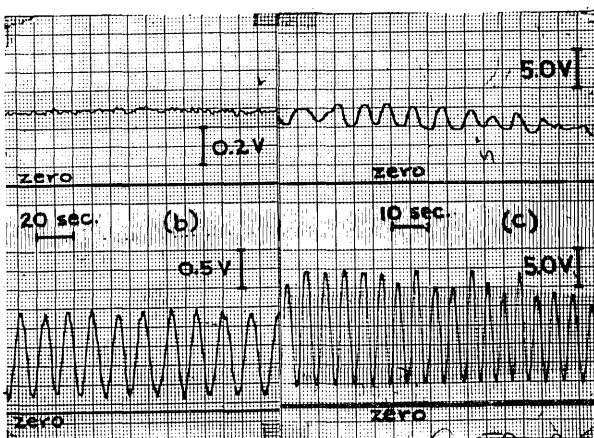
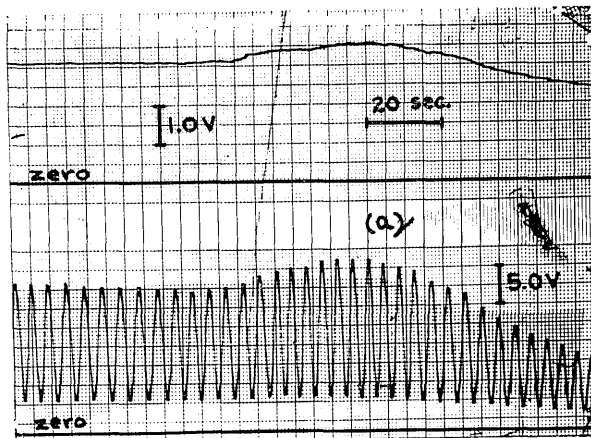


FIG. 8. Some sample recordings obtained with the WAMI. The upper trace indicates the source radiance as obtained by the monitor photometer. (a) A scan across an auroral form, (b) nightglow, and (c) rapidly fluctuating aurora.